Journal of Solid State Chemistry 182 (2009) 312–316

Contents lists available at ScienceDirect

Journal of Solid State Chemistry

journal homepage: www.elsevier.com/locate/jssc

# Preparation of porous $TiO_2$/silica composites without any surfactants

Suxia Ren, Xu Zhao, Lina Zhao, Meirong Yuan, Yang Yu, Yupeng Guo *, Zichen Wang

*College of Chemistry, Jilin University, Changchun 130023, China*

ARTICLE INFO

*Article history:*
Received 25 March 2008
Received in revised form
15 September 2008
Accepted 18 October 2008
Available online 5 November 2008

*Keywords:*
$TiO_2$/silica composites
Chemical synthesis
Catalytic properties

ABSTRACT

$TiO_2$–$SiO_2$ composites, with high specific surface area (up to 308 $m^2$/g), large pore volume, and narrow distribution with average pore sizes of 3.2 nm, have been synthesized from wollastonite and titanium sulfate in the absence of any surfactants. Calcium sulfate, a microsolubility salt, plays an important role in the formation of pores in this porous $TiO_2$/silica composite. The microstructure and chemical composition of composite were characterized by X-ray diffractometry (XRD), transmission electron microscopy (TEM) equipped with energy-dispersive X-ray spectroscopy (EDX), X-ray photoelectron spectrometer (XPS) and $N_2$ adsorption and desorption analysis. The as-prepared porous titanium dioxide–silicon dioxide composites with high specific surface area and well-crystallized anatase contents were used as an efficient photocatalyst.



## 1. Introduction

Titanium dioxide ($TiO_2$), as an important photocatalyst, has been employed for decomposing organic pollutants in aqueous systems and in air [1–4]. The specific surface areas and polymorphs of the photocatalyst are the key effect factors of photocatalytic activity. Pure ultrafine powders will agglomerate into larger particles, resulting in an adverse effect on catalyst performance [5]. So various strategies have been used to accept large $TiO_2$ surface areas, such as $TiO_2$ mesoporous molecular sieves, $TiO_2$ pillared clays, and titania–silica mixed oxides. For the first strategy, although many cases of the synthesis of porous titania have been reported, there were a few reports on the synthesis of stable porous titania with a crystalline wall that had a high photocatalytic activity [5–8]. $TiO_2$ pillared clays were used to achieve large specific surface areas. Some of them were only simple mixing of titania and clay mineral dispersions [9] and these $TiO_2$ pillared clays were amorphous [10]. The layered silicates were also used [5,11] to achieve large specific surface area in the presence of surfactant [5]. All of these methods limited the applications of materials.

Titania–silica materials had been widely used as photocatalysts, acid catalysts, and oxidation catalysts, recently [12–14]. The catalytic function of titania–silica was mainly attributed to $TiO_2$, and $SiO_2$ had high thermal stability and excellent mechanical strength. The addition of silica can both enhance the dispersion of titania and improve the activity of $TiO_2$ [15,16]. To our knowledge, there were few reports on the synthesis of porous titania–silica nanocomposite from raw minerals without any surfactant.

In this work, we succeeded in preparing $TiO_2$–$SiO_2$ composite with high specific surface area and narrow pore size distribution from cheap materials by chemical deposition method and a potential photocatalytic application of this composite was also carried out using the photo oxidation of a dye, methyl orange, as probe reaction. No surfactant was used in this reaction system, and the calcium sulfate that formed in the reaction process played an important role in the formation of pores in composite. This new synthesis route is a simple, cost effective for large scale production of titania–silica composite photocatalyst.

## 2. Experimental

### 2.1. Preparation of $TiO_2$–$SiO_2$ composites

The reagents used were titanium (IV) sulfate (A.R. grade) and commercial wollastonite powder (main substance: $CaSiO_3$, average particle size 50 μm). All compounds were used as received without further purification. Typically, $TiO_2$–wollastonite composites were prepared in the following way: 1.16 g wollastonite were added into 100 ml, 0.1 mol/L titanium sulfate aqueous solution with constant stirring at ambient temperature, incubation for more than 24 h. Then the suspension was subjected to hydrothermal treatment of 80 °C for 3 h. Then the sediment was centrifugated and washed with plenty of deionized water until it was free of $SO_4^{2-}$ anions according to the test of $BaCl_2$. At last the product was dried at 80 °C for 12 h and calcined at different temperature.

* Corresponding author. Fax: +86 431 8499134.
*E-mail address:* guoyupeng@jlu.edu.cn (Y. Guo).

0022-4596/$ - see front matter © 2008 Elsevier Inc. All rights reserved.
doi:10.1016/j.jssc.2008.10.027

### 2.2. Photocatalytic experiment

The evaluation of photocatalytic activity was carried out by the degradation of methyl orange using a beaker made of Pyrex glass equipped with a magnetic stirring bar. For irradiation experiments, 500 ml solution of methyl orange of 50 mg/L concentration was taken into the vessel and required amount of the catalyst (1 g/L) was added into the solution. Before irradiation, the solution was magnetically stirred for 30 min to allow the equilibration of the system so that the loss of compound due to the adsorption can be considered. The degradation rate for the decomposition (decrease in absorption intensity vs. irradiation time) of methyl orange under investigation was monitored by measuring the change in absorbance on a UV-Vis spectrophotometer (Scinco). The absorbance of the methyl orange was followed at 490 nm wavelength. For each experiment, the rate constant was calculated from the initial slope obtained by linear regression from a plot of the natural logarithm of the absorbance of the dye as a function of irradiation time.

### 2.3. Characterization methods

Powder X-ray diffraction (XRD) patterns of the samples were taken on an SHIMADZU-6000 X-ray diffractometer, with Cu$K\alpha$ ($\lambda = 1.54056$ Å) radiation being used at 40 kV and 30 mA. The transmission electron microscopy (TEM) images were obtained by means of HITACHI (H-8100) TEM equipped with energy-dispersive X-ray spectroscopy (EDX), using an accelerating voltage of 100 kV. The $N_2$ adsorption measurements were performed at 77 K, using a QUANTACEROME AUTOSORB-1C analyzer and utilizing Barrett–Emmett–Teller (BET) calculations for surface area and BJH calculations for pore size distribution for the desorption branch of the isotherm. The XPS analysis of the samples was carried out in an ESCALAB MARK II (VG Scientific) photoelectron spectrometer. The photoelectrons were excited with an X-ray source using Al$K\alpha$ ($h\upsilon = 1486.3$ eV). To correct the measured values of binding energy (BE) for the charging effect, all spectra were calibrated to adjust BE (C1*s*) to 284.4 eV.

## 3. Results and discussion

The XRD patterns of the starting wollastonite and the obtained $TiO_2$–$SiO_2$ composites are shown in Fig. 1. The pattern of pristine wollastonite (Fig. 1a) could be perfectly indexed to 1Tr-type $CaSiO_3$, which is in agreement with JCPDS 271064. When wollastonite were pretreatment for 24 h with titanium sulfate, new peaks occurred. These peaks around 20, 29, and 31 were assigned to $CaSO_4$ (Fig. 1b). After pretreatment, the samples were subjected to hydrothermal treatment, the XRD pattern of washed and unwashed sample were shown in Figs. 1c and d. It can be seen form Fig. 1c that the diffraction peaks of $CaSO_4$ still exist for the unwashed sample, while all the $CaSO_4$ diffraction peaks disappeared after carefully washing. Characteristic diffraction peaks for anatase with *d*-spacings of 3.52, 2.38, 1.89, and 1.69 Å ($2\theta$ values: 25.3°, 37.8°, 48.0°, and 54.4°, respectively) can be clearly observed from the XRD pattern of the sample (Fig. 1d enlargement), the reflections can be indexed to pure anatase phase of $TiO_2$ conforming to a space group of $I4_1/amd$ (141) (JCPDS 841285). It means that the anatase phase has formed during aging process. The hydrothermal-induced crystalline anatase formation manifested itself in the broadening of the XRD peaks at $2\theta$ of about 25.3°. Taking advantage of this broadening, we estimated the diameters of the crystalline anatase in $2\theta = 25.3^\circ$ to be 4.2 nm using the Warren–Averbach method [17].

Transmission electron micrographic image (as shown in Fig. 2) indicated that the $TiO_2/SiO_2$ composites were in nanometer scale.

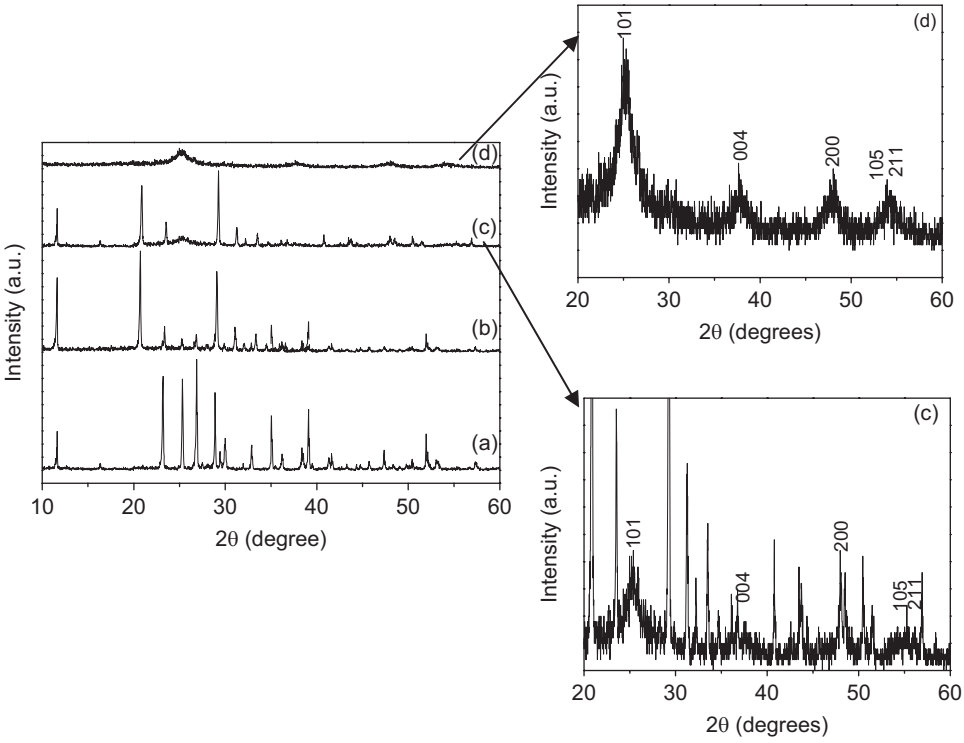


**Fig. 1.** Powder XRD patterns for samples: (a) wollastonite, (b) the sample after pretreatment, (c) the composite without washing carefully, and (d) the obtained $TiO_2$–$SiO_2$ composites. And the enlargements of (c) and (d) are shown right.

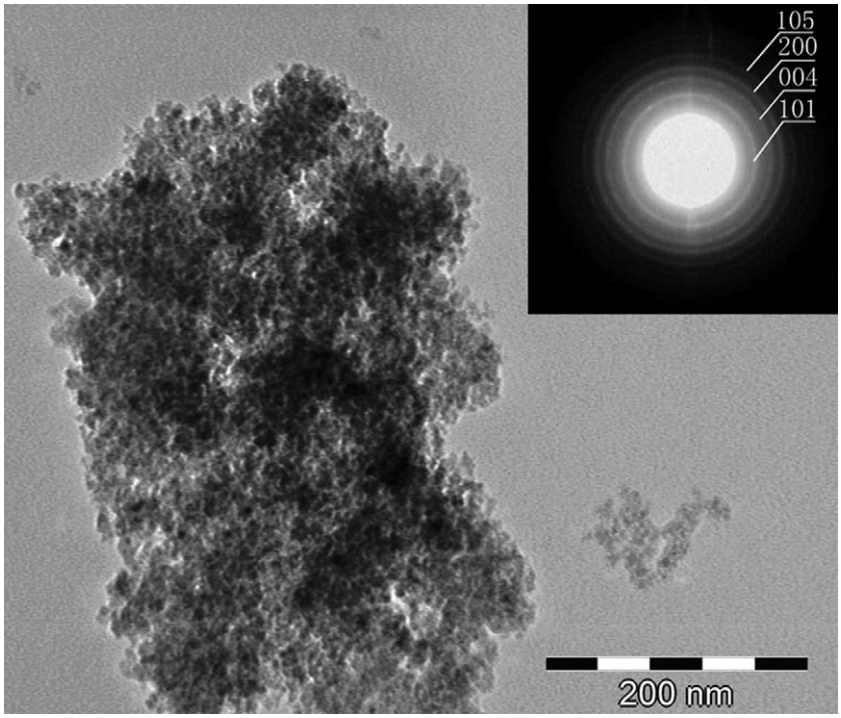


**Fig. 2.** TEM image of obtained $TiO_2$–$SiO_2$ composites and electron diffraction of composites (inset).

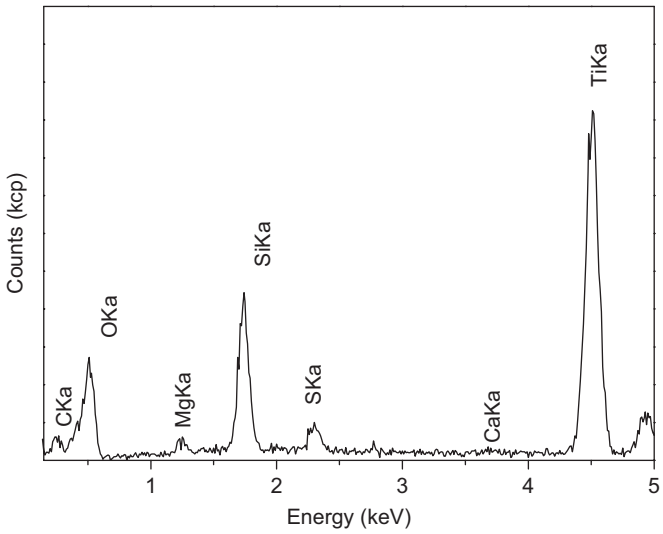


**Fig. 3.** The energy-dispersive X-ray spectroscopy (EDX) data of $TiO_2$–$SiO_2$ composites.

The electron diffraction picture of the nanocomposite was shown in Fig. 2 (inset), it showed clearly that the $TiO_2$ particles are predominantly in the anatase form, which agrees with the XRD result. The EDX data in Fig. 3 displays that major elements Si, Ti, and O are detected. Trace amount of Mg and S came from the materials used in sample preparation. No calcium element was detected, which indicated that a complete removal of calcium ions by washing with deionized water and the sample was $TiO_2/SiO_2$ composite.

To clarify the existence of Ti–O–Si bonds in nanocomposites, the XPS (it can distinguish the chemical situations of the elements) of the sample was measured. As is shown in Fig. 4a, the BE of Ti $2p_{3/2}$ is 458.8 eV, which is consistent with the reported value of $TiO_2$ (458.4 [16] and 458.7 eV with a standard deviation of 1.3 eV [18]). Also, the XPS profile of O1*s* is shown in Fig. 4b. The profile can be deconvoluted to three peaks, 530.0, 533.1, and 531.5 eV, which can be attributed to Ti–O–Ti, Si–O–Si, and Si–O–Ti bonds, respectively [12,16]. As a result, new bonds have formed in the preparation process.

On the basis of a series of experiments, the formation of the $TiO_2$/silica composites can be explained as follows (Fig. 5): (1) Because the $Ti(SO_4)_2$ is highly sensitive to $H_2O$, it is possible for $Ti(SO_4)_2$ to hydrolyze and form $H^+$ and titanium species. (2) In acid $Ti(SO_4)_2$ solution, Ca and Si ions in chain-like wollastonite could dissolve into the bulk solution and slightly soluble $CaSO_4$ crystal phase and silicic acid formed. (3) Since the concentration of the titanium species in the reaction solution is expected to increase with the hydrolysis process, nucleation starts. After the start of the nucleation, a very small amount of $TiO_2$, silicate and $CaSO_4$ particle deposited together and formed composites. (4) Some cavities formed during the washing step through the dissolution of $CaSO_4$ crystal phase. The bulk of the material is then transformed from wollastonite into TiO2/silica composites.

The calcination temperature may have significant effect on the phase, BET surface area and other properties of the samples which in turn regulate the photocatalytic properties of the samples. Hence, this sintering effect had been studied through the calcination process at temperature from 300 to 800 °C for 2 h. Changes in phase and morphology was followed by XRD and BET analyses.

Fig. 6 shows the XRD patterns of samples calcined at various temperatures. It can be seen from the figure that the intensity of the XRD profiles increases with sintering temperature increasing. The patterns were more or less similar except that the intensity of diffraction peak near $2\theta = 25^\circ$ was increased. The average grain size of the composite estimated from the XRD profiles using the Warren–Averbach method is about 4.2, 4.5, 5.2, and 12.3 nm. The size increased with the sintering temperature.

The effect of heat treatment at different temperatures on the $N_2$ adsorption and desorption isotherms of nanocomposites was

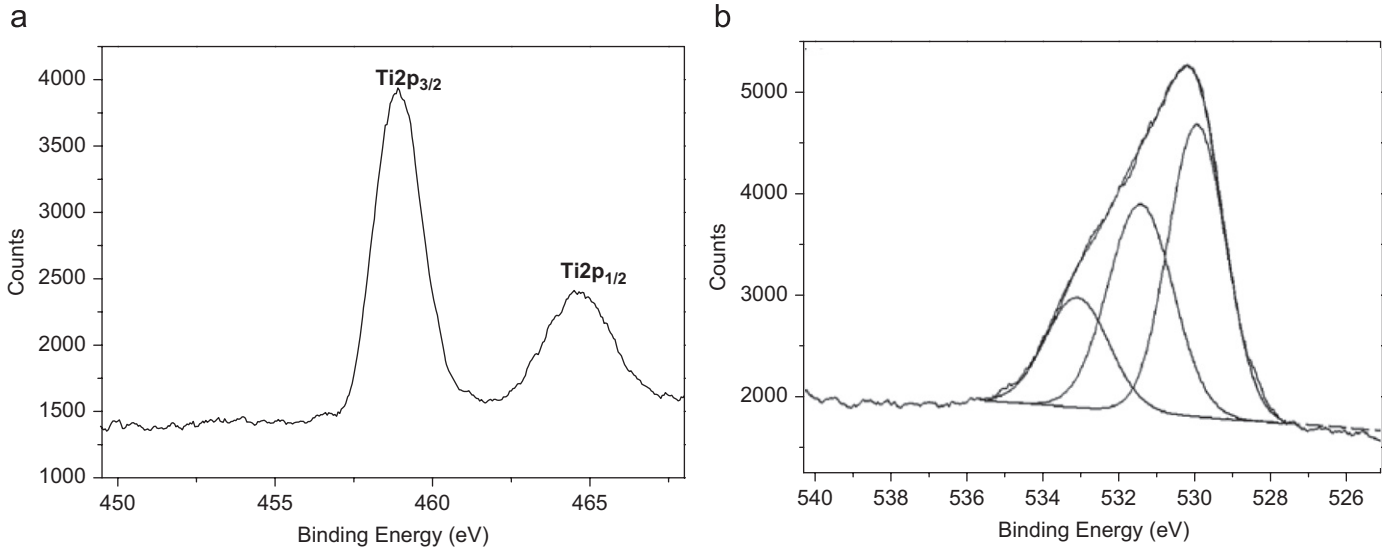


**Fig. 4.** The X-ray photoelectron spectrometer (XPS) spectra of $TiO_2$–$SiO_2$ composites: (a) Ti2*p* and (b) O1*s*.

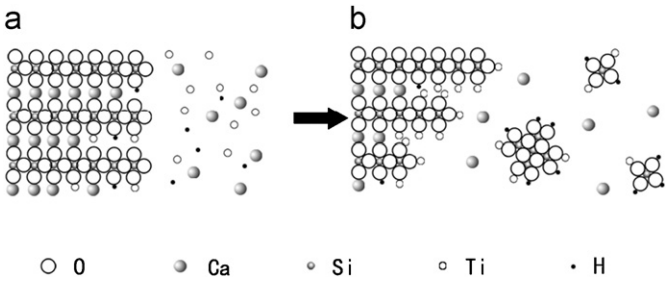


**Fig. 5.** Simplified schematic diagram of the reaction mechanism.

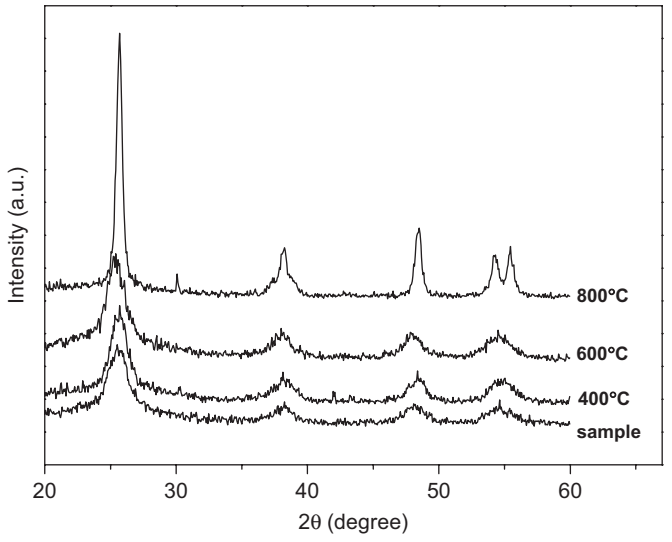


**Fig. 6.** The XRD patterns of samples calcined at different temperatures.

studied and depicted in Fig. 7. In particular, the sample without calcination process showed a nitrogen adsorption capacity of 0.25 ml/g with a specific BET surface area of 308 $m^2$/g. The average pore diameter was about 3.2 nm (shown in Fig. 4b). However, the unwashed sample had a very low specific BET surface area (85.2 $m^2$/g) for the component of $CaSO_4$ still existed in the composite. When washed out with deionized water, new cavities occurred and these cavities leaded to the generation of pores in the composites. Here, $CaSO_4$ played a role as a surfactant which is used in the porous material preparation process.

The specific surface area of the calcined samples was found to be strongly influenced by heat treatment. The specific surface area showed distinct values depending on sintering temperature and was 308, 264, 185, and 99 $m^2$/g, respectively. The specific surface area was sharply decreased at higher temperature. The corresponding BJH pore size distributions of the samples calcined at different temperature were shown in Fig. 4b. It can be seen that the pore size increased with the calcined temperature increasing, and the pore size distribution of the sample calcined at 800 °C is broader than that of sample calcined at 400 °C. As mentioned above, these changes may be attributed to different factors, such as sintering effect and growth of crystallites.

The photocatalytic activity of the as prepared sample and their thermal derivatives has been evaluated using the photooxidation of methyl orange as probe reaction (shown in Fig. 8). It can be seen that the sample calcined at 400 °C has the highest photocatalytic activity, and the sample calcined at 800 °C has the lowest photocatalytic activity, it may be caused by the decrease of BET surface area. Although the sample without further calcination process has the largest specific surface area, it photocatalytic activity was poor. Low photocatalytic activity compared of the calcined samples could be due to poor degree of crystallinity.

## 4. Conclusions

In the present work, mesoporous $TiO_2$–$SiO_2$ nanocomposites with high special surface areas and narrow distribution of pore sizes were prepared from wollastonite and titanium sulfate in the absence of any surfactants. This method provides a facile approach to synthesize titania–silica porous composites with high special surface areas. It was found that the as-prepared $TiO_2$–$SiO_2$ nanocomposites had high specific surface areas and well-crystallized anatase contents, and could be used as an efficient photocatalyst.

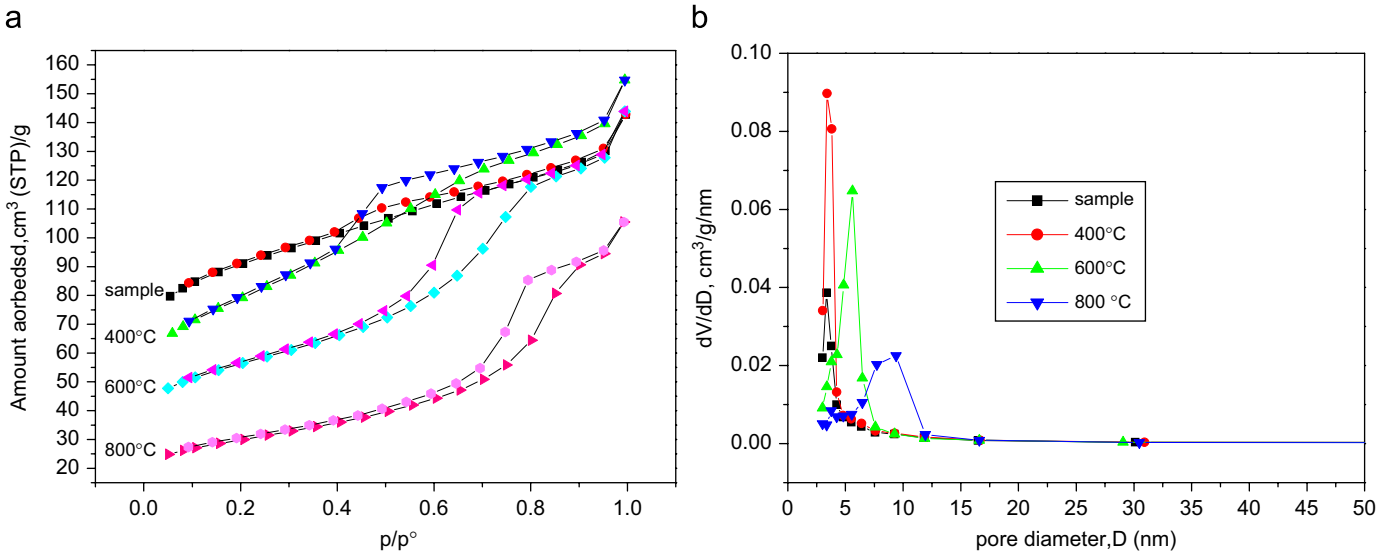


**Fig. 7.** (a) $N_2$ adsorption and desorption isotherms of nanocomposites and (b) corresponding BJH pore size distribution curve determined from the $N_2$ desorption isotherm.

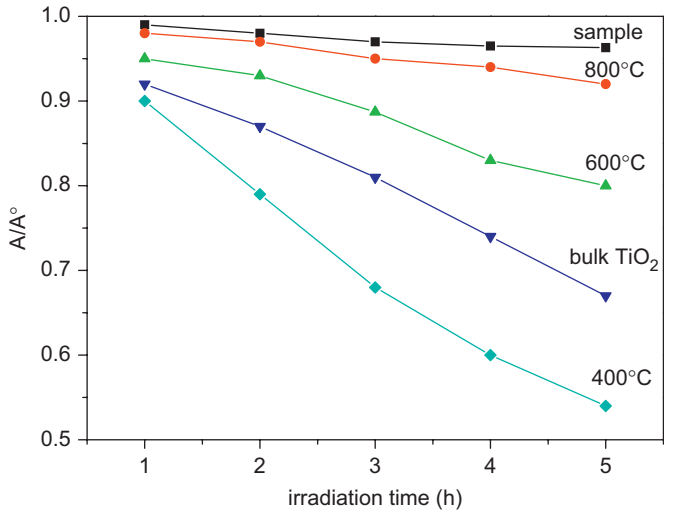


**Fig. 8.** Photocatalytic degradation of methyl orange in the presence of sample calcined at different temperatures for 2 h.

## Acknowledgment

The work was financially supported by the Doctor Start Research Foundation of Jilin University (No. 420010302323).

## References

[1] M. Addamo, V. Augugliaro, A.D. Paola, E. García-López, V. Loddo, G. Marcí, R. Molinari, L. Palmisano, M. Schiavello, J. Phys. Chem. B 108 (2004) 3303.
[2] J. Zhu, J. Zhang, F. Chen, M. Anpo, Mater. Lett. 59 (2005) 3378.
[3] G. Liu, X. Li, J. Zhao, H. Hidaka, N. Serpone, Environ. Sci. Technol. 34 (2000) 3982.
[4] M. Anpo, Pure Appl. Chem. 72 (2000) 1265.
[5] H.Y. Zhu, J.A. Orthman, J.-Y. Li, J.-C. Zhao, G.J. Churchman, E.F. Vansant, Chem. Mater. 14 (2002) 5037.
[6] P. Yang, D. Zhao, D.I. Margolese, B.F. Chmelka, G.D. Stucky, Nature 396 (1998) 152.
[7] T. Peng, A. Hasegawa, J. Qiu, K. Hirao, Chem. Mater. 15 (2003) 2011.
[8] P.C.A. Alberius, K.L. Frindell, R.C. Hayward, E.J. Kramer, G.D. Stucky, B.F. Chmelka, Chem. Mater. 14 (2002) 3284.
[9] Z. Ding, H.Y. Zhu, P.F. Greenfield, G.Q. Lu, J. Colloid Interface Sci. 238 (2001) 267.
[10] Z. Ding, H.Y. Zhu, G.Q. Lu, P.F. Greenfield, J. Colloid Interface Sci. 209 (1999) 193.
[11] K. Mogyorósi, I. Dékány, J.H. Fendler, Langmuir 19 (2003) 2938.
[12] X. Gao, I.E. Wachs, Catal. Today 51 (1999) 233.
[13] Y. Li, S.J. Kim, J. Phys. Chem. B 109 (2005) 12309.
[14] R.V. Grieken, J. Aguado, M.J. López-Muñoz, J. Marugán, J. Photochem. Photobiol. A 148 (2002) 315.
[15] T.C. Liu, T.I. Cheng, Catal. Today 26 (1995) 71.
[16] H. Zhang, X. Luo, J. Xu, B. Xiang, D. Yu, J. Phys. Chem. B 108 (2004) 14866.
[17] R.N. Viswanath, J. Phys. Chem. Solids 62 (2001) 1991.
[18] U. Diebold, T.E. Madey, Surf. Sci. Spectra (4) (1998) 227.